nature nanotechnology

SUPPLEMENTARY INFORMATION

DOI: 10.1038/NNANO.2014.260

Light-powered autonomous and directional molecular motion of a dissipative self-assembling system

Giulio Ragazzon, Massimo Baroncini, Serena Silvi, Margherita Venturi and Alberto Credi*

Table of Contents

1. General Methods

Materials and Characterization Methods. Compound **1** was synthesized according to previously published procedures[1]. Compounds *E*-$\mathbf{2}^+$, $\mathbf{3}^+$ and *EE*-$\mathbf{4}^+$ were available from previous investigations[2]. Solvents were dried according to literature procedures. The ^{1}H and ^{13}C NMR spectra were recorded at 298 K in CD_2Cl_2 with a Varian Mercury 400 spectrometer with the deuterated solvent as the lock and the residual solvent as the internal standard.

UV-Visible Spectroscopy and Photochemistry. Absorption spectra were recorded with a Varian Cary 50Bio, Agilent Technologies Cary 300 and Perkin Elmer Lambda45 spectrophotometers, on air equilibrated CH_2Cl_2 (Romil) solutions at room temperature (ca. 20°C), with concentrations ranging from 1×10^{-5} to 1×10^{-3} M. Solutions were examined in 1-cm spectrofluorimetric quartz cells. Dedicated spectrophotometric cells endowed with two compartments separated by a quartz wall were employed for a careful determination of the sum of the absorption spectra of the separated components (unmixed solutions) and the absorption spectrum of their complex (mixed solutions). The experimental error on the wavelength values was estimated to be ±1 nm. Photochemical reactions were performed on CH_2Cl_2 solutions at room temperature (ca. 20°C), thoroughly stirred and eventually argon-purged (if irradiated for more than typically 1 h), by using a Hanau Q400 or Helios Italquartz Polymer 125 medium pressure Hg lamp (respectively 150 and 125 W); ^{1}H NMR photochemical isomerization experiments were performed in air equilibrated CD_2Cl_2 solutions irradiated directly inside the NMR tube. The selection of the desired irradiation wavelength (287, 365 or 436 nm) was accomplished by the use of an appropriate interference filter. The number of incident photons, determined by ferrioxalate actinometry in its micro version[3], was 2.4×10^{-8} Einstein min^{-1} at 287 nm, 1.0×10^{-7} Einstein min^{-1} at 365 nm, and 2.4×10^{-7} Einstein min^{-1} at 436 nm. The $E\rightarrow Z$ photoisomerization quantum yield (λ_{irr}= 365 nm) was determined from the disappearance of the $\pi\pi^*$ absorption band of the azobenzene unit of the reactant at low conversion percentages (<10%; extrapolation to t=0 was made). The fraction of light transmitted at the irradiation wavelength was taken into account in the calculation of the yields. The experimental error on the quantum yield values was estimated to be ±10%.

UV-Visible Spectroscopic Measurements. Reaction kinetic profiles were collected on air-equilibrated CH_2Cl_2 (Romil) solutions at 20°C. Threading processes were investigated by monitoring the time-dependent spectroscopic changes observed after addition of a concentrated (typically mM) solution of the axle to a more diluted ring solution. Dethreading reactions were triggered by dilution and were studied by monitoring the time-dependent spectroscopic changes observed after rapid mixing of the investigated complex with the solvent. Thermal $Z\rightarrow E$

isomerization reactions were performed at 20°C in the dark, monitoring the time-dependent absorption changes with a spectrophotometer. In all cases the data were elaborated by means of the SPECFIT fitting program[4]. Threading processes were modeled according to a mixed-order scheme, that is, second order (threading) and first order (dethreading) opposing reactions (equation S1)

$$\mathbf{1} + \text{Guest} \underset{k_{\text{out}}}{\overset{k_{\text{in}}}{\rightleftarrows}} [\mathbf{1}\supset\text{Guest}] \qquad \text{(S1)}$$

Dethreading processes and thermal $Z{\rightarrow}E$ isomerization reactions were modelled according to first-order kinetics. The values reported in Table 1 are typically an average of at least 3 independent experiments. The estimated experimental error for k_{in} values is ±20%; consequently, the error on the threading energy barriers is $\delta\Delta G^{\ddagger}_{\text{in}} \approx RT\ \delta k_{\text{in}}/k_{\text{in}} = 0.20RT \approx 0.12$ kcal mol^{-1} at 20°C. As for the dethreading rate constants, $\delta k_{\text{out}}/k_{\text{out}} = [(\delta k_{\text{in}}/k_{\text{in}})^2 + (\delta K/K)^2]^{½} \approx \pm30\%$; the error on the dethreading energy barriers is $\delta\Delta G^{\ddagger}_{\text{out}} \approx RT\ \delta k_{\text{out}}/k_{\text{out}} = 0.30RT \approx 0.18$ kcal mol^{-1} at 20°C.

Spectroscopic titrations. Stability constants were determined from titration curves obtained by measuring the luminescence intensity of **1** ($\lambda_{\text{exc}} = 272$ nm) upon addition of small aliquots of a concentrated solution of the considered guest to 2.5 mL of a dilute solution (typically, 50 μM) of **1** in CH_2Cl_2 at 20°C. To minimize inner filter effects, the emission detection was performed on isosbestic point (390 nm). In the case of the $[\mathbf{1}\supset\mathbf{3}]^+$ complex, the absorbance changes at 325 nm were used to obtain the binding isotherm, because the luminescence intensity of **1** is not affected by addition of $\mathbf{3}^+$. In all cases the constants were calculated by means of the SPECFIT fitting program according to a 1:1 binding model[4]. The estimated experimental error on K values is ±20%; consequently, the error on the free energy change values is $\delta\Delta G° \approx RT\ \delta K/K = 0.20RT \approx 0.12$ kcal mol^{-1} at 20°C.

Microscopic reversibility considerations. For a square network of chemical reactions such as that represented in Fig. S1, microscopic reversibility imposes that when the cycle is at thermodynamic equilibrium each individual process must be equilibrated and its net rate must be zero ($v_1 = v_2 = v_3 = v_4 = 0$). The equilibrium constant of reaction A⇆B must correspond to the product of the equilibrium constants of reactions A⇆D, D⇆C and C⇆B. In other words, $K_1 = K_4 \times K_3 \times 1/K_2$, or

$$K_1/K_3 = K_4/K_2 \qquad \text{(S2)}$$

It should be noted that equation (S2) is not strictly valid when photochemical reactions are involved, as microscopic reversibility does not apply. However, the observation of a behaviour deviating from equation (S2) for the cycle shown in Fig. 3 (or Fig. S2 below) can be taken as an experimental evidence that the system does not fulfil detailed balance.

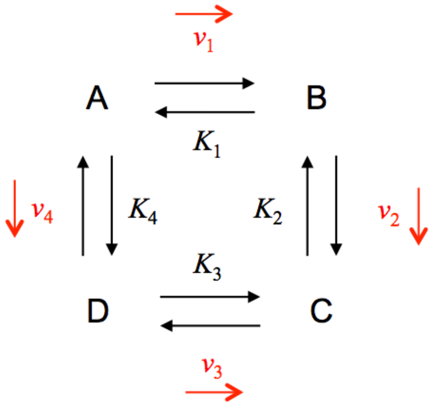

Supplementary Fig. 1. Square cycle consisting of four chemical equilibria. The indicated parameters refer to the reactions read from left to right and from top to bottom. Detailed balance states that, at equilibrium, all net rates are zero.

Kinetic modelling. The modelling of the kinetic behaviour of the system was performed by means of the SPECFIT software[4]. The mechanism used to simulate the experimental behaviour is depicted in Fig. S2 below and corresponds to that shown in Fig. 3.

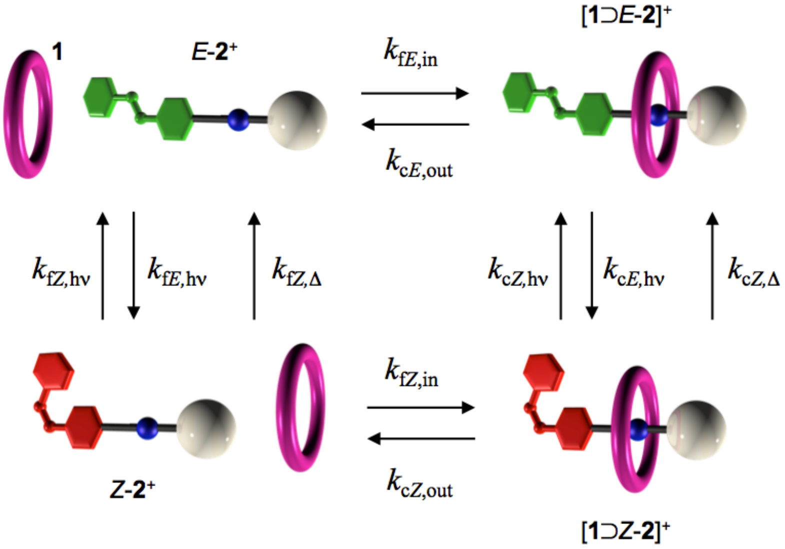

Supplementary Fig. 2. Kinetic scheme used to simulate the experimental behaviour. Photo and thermal *Z*→*E* isomerization processes - here shown as separate processes for clarity - will be modelled by a single cumulative rate constant (see text for details).

Indexes f and c denote free and complexed axles, respectively, whereas hν and Δ indicate photoisomerization and thermal isomerization reactions, respectively. The threading and dethreading processes are modelled as bimolecular and unimolecular processes, respectively; the corresponding rate constants are second-order (k_{in}) and first-order (k_{out}) constants. $Z \rightarrow E$ Thermal isomerization processes (Δ) are unimolecular processes. Under the employed experimental conditions (irradiation with monochromatic light and low absorbance at the irradiation wavelength), photoisomerization reactions (hν) can be treated as unimolecular processes. In fact, the photoisomerization quantum yield is expressed as:

$$\Phi = -\frac{\Delta C\ V}{N_{\mathrm{h}\nu}} \tag{S3}$$

in which ΔC is the concentration change corresponding to the disappearance of the reactant (e.g., the E form for the $E \rightarrow Z$ photoisomerization) in a given time interval, V is the volume of the irradiated sample and $N_{\mathrm{h}\nu}$ is the number of photons absorbed by the reactant in the same time interval. Such a number is the product of the photon flow ($F_{\mathrm{h}\nu}$), the fraction of light absorbed at the irradiation wavelength ($\Im_{\mathrm{irr}}$) and the time interval (Δt):

$$N_{\mathrm{h}\nu} = F_{\mathrm{h}\nu}\ \Im_{\mathrm{irr}}\ \Delta t = F_{\mathrm{h}\nu}\ (1 - 10^{-A_{\mathrm{irr}}})\ \Delta t \tag{S4}$$

The exponential term in equation (S4) can be expanded and, if the absorbance at the irradiation wavelength is reasonably low (typically <0.1), orders higher than 1 can be neglected[5]. Hence,

$$N_{\mathrm{h}\nu} \approx F_{\mathrm{h}\nu}\ A_{\mathrm{irr}}\ \Delta t = F_{\mathrm{h}\nu}\ \varepsilon_{\mathrm{irr}} b\ C\ \Delta t \tag{S5}$$

in which $\varepsilon_{\mathrm{irr}}$, b and C are the molar absorption coefficient of the reactant at the irradiation wavelength, the optical path length and the reactant concentration. Substitution in equation (S3) yields equation (S6):

$$\Phi = -\frac{\Delta C\ V}{F_{\mathrm{h}\nu} \varepsilon_{\mathrm{irr}} b\ C\ \Delta t} \tag{S6}$$

which, after rearrangement, results in equation (S7).

$$-\frac{\Delta C}{\Delta t} = \frac{\Phi\ F_{\mathrm{h}\nu}\ \varepsilon_{\mathrm{irr}} b\ C}{V} = k\ C \tag{S7}$$

showing that the photoreaction obeys a first order kinetic law.

The values of the parameters related to chemical equilibria used in the simulation correspond to the experimental ones reported in Table 1 and Table S1. The apparent first-order rate constant for the $E\rightarrow Z$ photoisomerization processes of the free ($k_{\mathrm{f}E,\mathrm{h}\nu}$) and complexed ($k_{\mathrm{c}E,\mathrm{h}\nu}$) axles were estimated from the photoisomerization quantum yield (determined from photochemical experiments), the photon flow (Einstein s^{-1}, measured by chemical actinometry), the molar absorption coefficient (determined from the absorption spectra), the irradiated volume (3 mL) and the optical path length (1 cm), according to equation (S7). They resulted to be $k_{\mathrm{f}E,\mathrm{h}\nu} = 1.5\times10^{-3}\ \mathrm{s}^{-1}$ and $k_{\mathrm{c}E,\mathrm{h}\nu} = 1.8\times10^{-3}\ \mathrm{s}^{-1}$. Upon optimization of the fitting, the value of $k_{\mathrm{f}E,\mathrm{h}\nu}$ was adjusted to $1.6\times10^{-3}\ \mathrm{s}^{-1}$ (well within experimental error). The cumulative apparent first-order rate constant of the $Z\rightarrow E$ photochemical and thermal isomerization processes (e. g., for the free axle, $k_{\mathrm{f}Z} = k_{Z,\mathrm{h}\nu} + k_{\mathrm{f}Z,\Delta}$) were estimated from the composition of the photostationary state, taking advantage of equation (S8) valid at the PSS[6]:

$$\frac{\varepsilon_E \Phi_{E\rightarrow Z}}{\varepsilon_Z \Phi_{Z\rightarrow E}} = \frac{[Z]_{\mathrm{PSS}}}{[E]_{\mathrm{PSS}}} \tag{S8}$$

Combination with equation (S7) yields

$$\frac{k_{\mathrm{f}E,\mathrm{h}\nu}}{k_{\mathrm{f}Z}} = \frac{[Z\text{-}\mathbf{2}^{+}]_{\mathrm{PSS}}}{[E\text{-}\mathbf{2}^{+}]_{\mathrm{PSS}}} \tag{S9}$$

$$\frac{k_{\mathrm{c}E,\mathrm{h}\nu}}{k_{\mathrm{c}Z}} = \frac{[\mathbf{1}\supset Z\text{-}\mathbf{2}^{+}]_{\mathrm{PSS}}}{[\mathbf{1}\supset E\text{-}\mathbf{2}^{+}]_{\mathrm{PSS}}} \tag{S10}$$

The resulting upper limiting values are $k_{\mathrm{f}Z} < 6.7\times10^{-5}\ \mathrm{s}^{-1}$ and $k_{\mathrm{c}Z} < 1.8\times10^{-5}\ \mathrm{s}^{-1}$. The thermal $Z\rightarrow E$ isomerization rate constants reported in Table S1 are lower limiting values for the same processes. Upon optimization of the fitting the value of $k_{\mathrm{f}Z}$ was adjusted within the experimental error to $8.0\times10^{-5}\ \mathrm{s}^{-1}$ and $k_{\mathrm{c}Z}$ was set equal to $1.8\times10^{-6}\ \mathrm{s}^{-1}$.

The simulation presented in Fig. 4 was obtained in three steps. First **1** and E-$\mathbf{2}^{+}$ were associated, without taking into account the equilibria involving light, i.e, the dark association of the components was simulated. Then, to reproduce the fast isomerization performed in the experiment, the obtained equilibrium concentrations for E-$\mathbf{2}^{+}$ and $[\mathbf{1}\supset E\text{-}\mathbf{2}]^{+}$ were mathematically converted to 96% Z-isomer. Finally, the simulation was performed taking into account all the rate constants described above; the emission intensity was obtained normalizing the concentration of free ring for its equilibrium value after the initial association of **1** and E-$\mathbf{2}^+$.

Energetic considerations. The free energy change of the system upon performing directional cycling can be calculated from equation (S11), in which the partition constant K is the ratio of the clockwise (P_{cw}) to counterclockwise (P_{ccw}) rates. This quantity corresponds to the maximum amount of energy that could in principle be converted into useful work. From the simulation of the experimental behaviour under our set of conditions we found that $P_{\mathrm{cw}}/P_{\mathrm{ccw}} = 160$; thus, at 20°C

$$\Delta G = -RT \ln K = -RT \ln \frac{P_{\mathrm{cw}}}{P_{\mathrm{ccw}}} = -3.0 \text{ kcal mol}^{-1} \tag{S11}$$

which corresponds to an energy of 5.1 $k_{\mathrm{B}}T$. This result is identical to that calculated by using the generalized fluctuation-dissipation theorem for a closed reaction cycle coupled to an external energy source[7,8].

Under the conditions employed, the cycling quantum yield is 2.3×10^{-3} moles einstein^{-1}, as calculated from equation (S12):

$$\Phi_{cycl} = \frac{N_{cycles}}{N_{h\nu}} = \frac{v_{cycl}\ \Delta t\ V}{F_{h\nu}(1-10^{-A_{\mathrm{irr}}})\ \Delta t} = 2.3\times10^{-3} \tag{S12}$$

where the number of cycles (N_{cycles}) performed in a given time interval (Δt) is calculated from the cycling rate ($v_{\mathrm{cycl}} = 1.7\times10^{-10}$ M s^{-1}) obtained from the kinetic simulation (see above). The number of photons absorbed ($N_{\mathrm{h\nu}}$) is given by equation (S3). It follows that, to perform a cycle under these conditions, ca. $1 / 2.3\times10^{-3} \approx 430$ photons of 365-nm light (78 kcal mol^{-1}) are needed on average. Therefore, the maximum energy conversion efficiency is

$$\eta_{\max} = \frac{\Delta E_{\max}}{Nh\nu} = \frac{3.0}{430\times78} = 9\times10^{-5} \tag{S13}$$

These figures show that the system is able to exploit only a tiny fraction of the input light energy because, perhaps not surprisingly, most of the energy is wasted into heat in excited-state vibrational relaxation processes.

2. NMR Spectroscopy

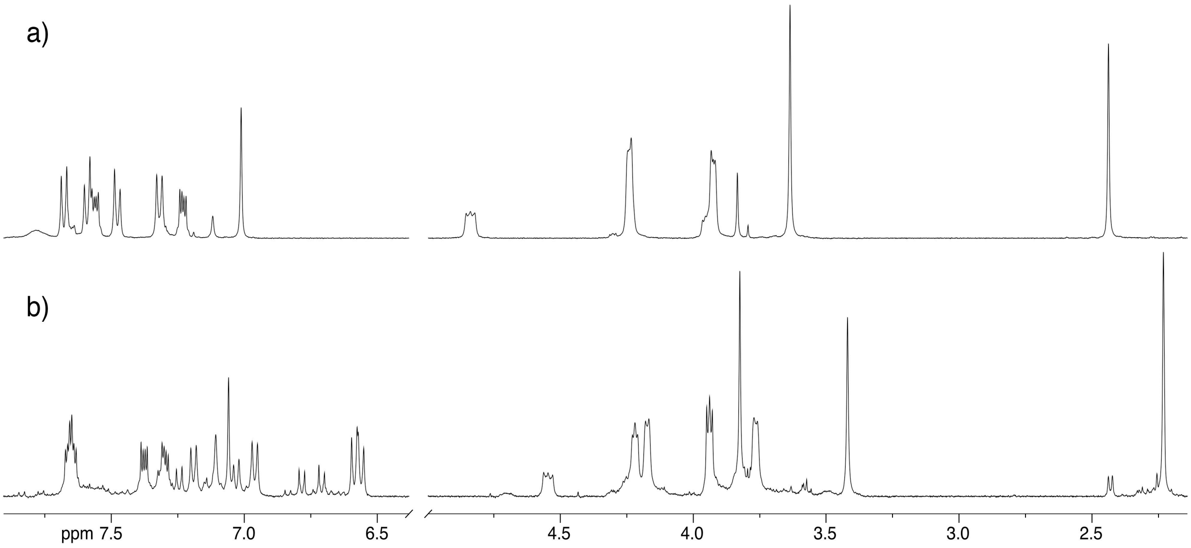

Supplementary Fig. 3. Partial ^{1}H NMR (400 MHz, CD_2Cl_2, 298 K) spectra of (a) a solution of **1** (3 mM) and [*EE*-**4**]PF_6 (3 mM) and (b) the same solution after exhaustive irradiation at λ = 365 nm.

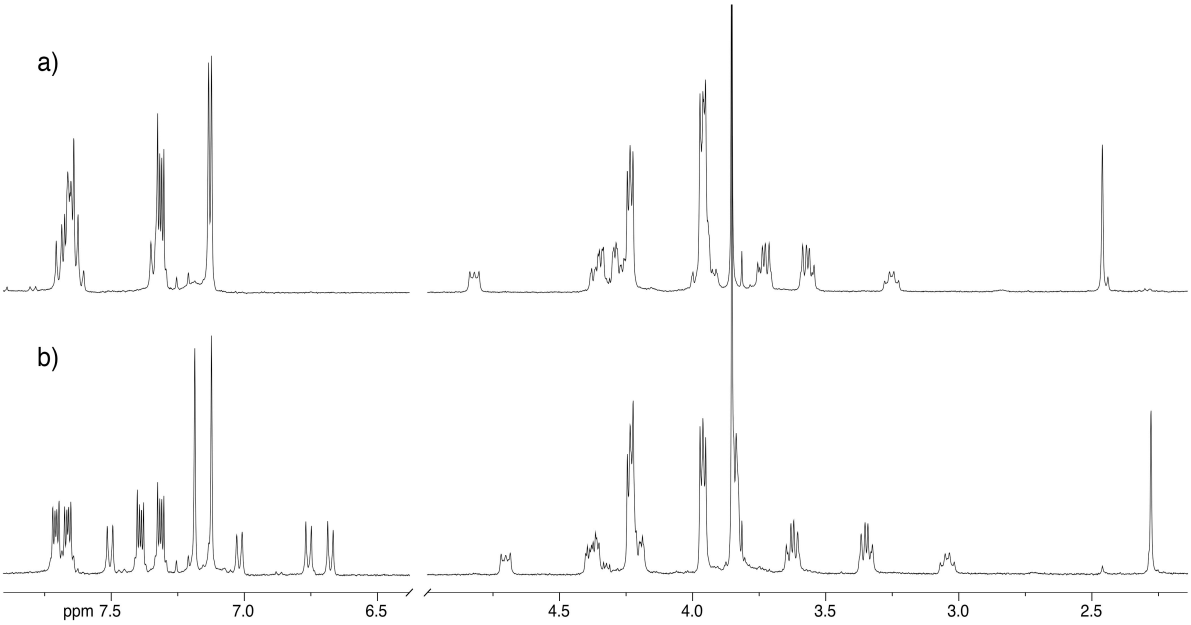

Supplementary Fig. 4. Partial ^{1}H NMR (400 MHz, CD_2Cl_2, 298 K) spectra of (a) a solution of **1** (3 mM) and [*E*-**2**]PF_6 (3 mM) and (b) the same solution after exhaustive irradiation at λ = 365 nm.

3. UV-Visible Spectroscopy

Supplementary Table 1. Spectroscopic and photochemical data of the investigated compounds (CH_2Cl_2, r.t.).

Compound	Absorption		Luminescence			Isomerization		
	λ_{max}, nm	ε, M^{-1} cm^{-1}	λ_{max}, nm	Φ_{em}	τ, ns	$\Phi_{E\to Z}$ (λ_{irr}, nm)	*Z/E* PSS, % (λ_{irr}, nm)	$k_{Z,\Delta}$, s^{-1}
1	268 324	9500 7900	343	0.26	9.8	—	—	—
E-**2**$^+$	332 448	23000 700	[a]	[a]	[a]	0.15 (365) 0.30 (346) 0.15 (287)	>96 (365)	—
[**1**⊃*E*-**2**]$^+$	323 448	30000 700	—	$<10^{-4}$	—	0.15 (365) 0.30 (436) 0.15 (287)	>99 (365)	—
Z-**2**$^+$	287 437	5500 1700	[a]	[a]	[a]	—	—	1.4×10^{-6} [b]
[**1**⊃*Z*-**2**]$^+$	323 437	9400 1700	—	$<10^{-4}$	—	—	—	1.3×10^{-6} [b]
3$^+$	[c]	[c]	[a]	[a]	[a]	—	—	—
[**1**⊃**3**]$^+$	268 322	9800 7600	343	0.26	—	—	—	—
EE-**4**$^+$	335 441	43000 1200	[a]	[a]	[a]	0.15 (365)	>96 (365)[d]	—
[**1**⊃*EE*-**4**]$^+$	323 441	46000 1200	—	$<10^{-4}$	—	0.15 (365) 0.15 (287)	>96 (365)[d]	—
ZZ-**4**$^+$	289 436	10000 2900	[a]	[a]	[a]	—	—	4×10^{-6} [b]
[**1**⊃*ZZ*-**4**]$^+$	—	—	—	$<10^{-4}$	—	—	—	—

[a] Not luminescent.

[b] Performed at 20 °C.

[c] The compound does not absorb in the investigated spectral region (250-800 nm).

[d] According to a statistical distribution of the *E* and *Z* azobenzene units, the composition of the PSS in terms of the various isomeric forms is 92% *ZZ*, 8% *EZ* and a negligible amount of *EE*.

Supplementary Table 2. Composition of the photostationary state for the free and complexed axle **2** under different irradiation conditions, determined from the disappearance of the $\pi\pi^*$ absorption band of the azobenzene unit of the axle.

λ_{irr} (nm)	*Z*-**2**$^+$ (%)	[**1**⊃*Z*-**2**]$^+$ (%)
287	24	31
365	96	>99
436	16	16

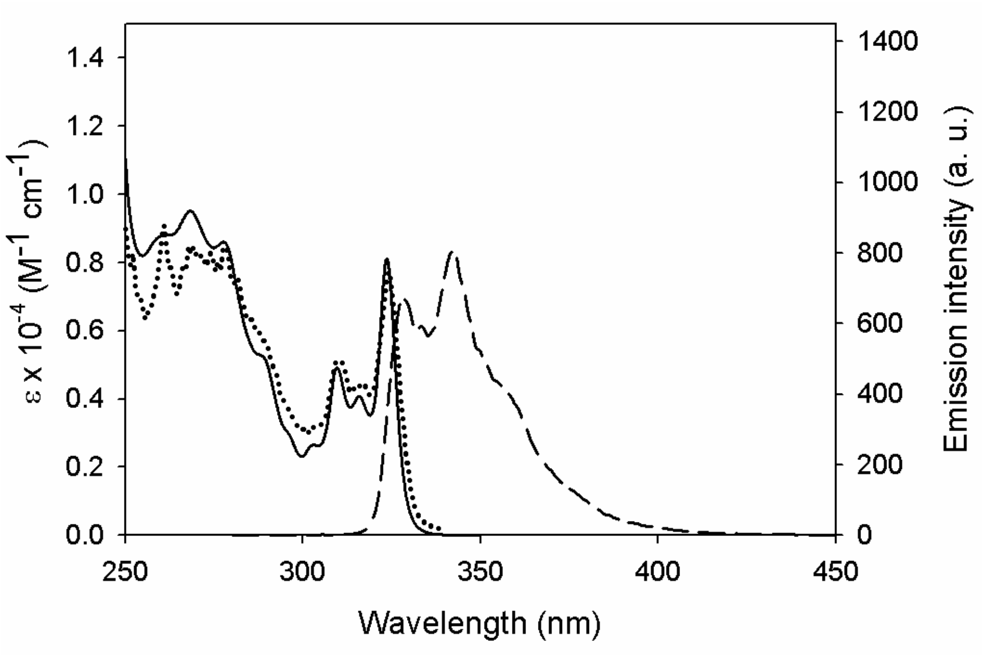

Supplementary Fig. 5. Absorption (full line, left scale) and luminescence (right scale) emission (dashed line, λ_{exc} = 272 nm) and excitation (dotted line, λ_{max} = 345 nm) spectra of macrocycle **1** (air equilibrated CH_2Cl_2, r.t.).

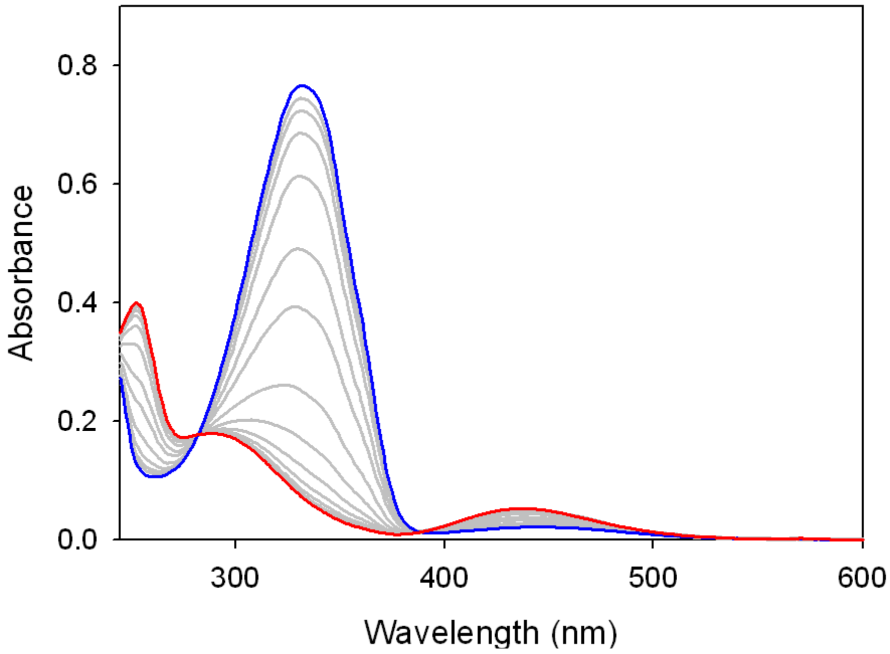

Supplementary Fig. 6. Absorption spectrum of 35 µM *E*-**2**$^+$ (blue line), and spectral changes observed upon irradiation of the solution at 365 nm, showing the occurrence of the *E*→*Z* photoisomerization (CH_2Cl_2, r.t.). The red line shows the absorption spectrum of *Z*-**2**$^+$.

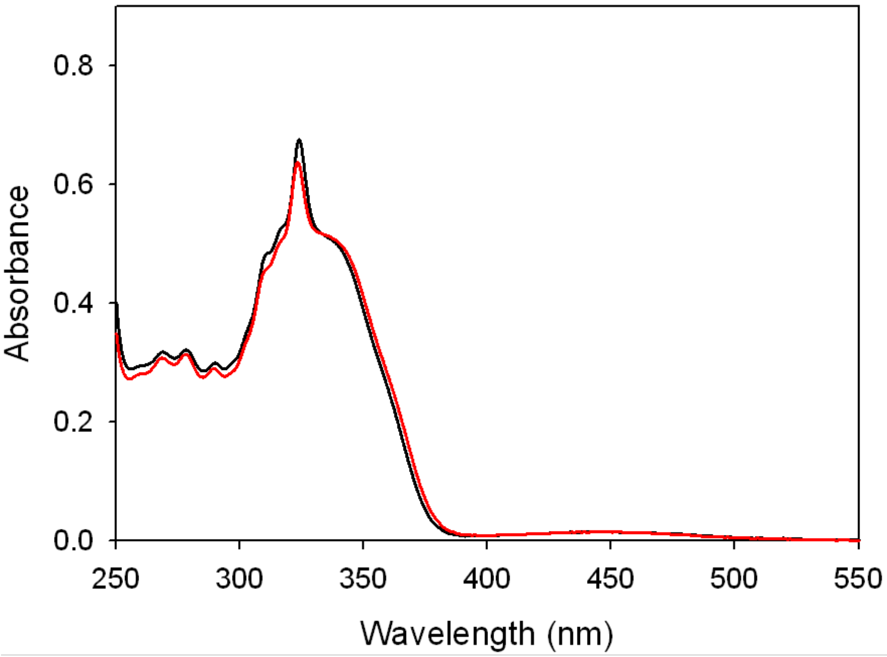

Supplementary Fig. 7. Sum of the absorption spectra of 20 μM **1** and *E*-$\mathbf{2}^+$ (black line), and absorption spectrum of the mixture of the two compounds (red line) at the same concentration (CH_2Cl_2, r.t.). Dedicated spectrophotometric cells with separated compartments allowed a careful *in situ* determination of the spectra of unmixed and mixed solutions.

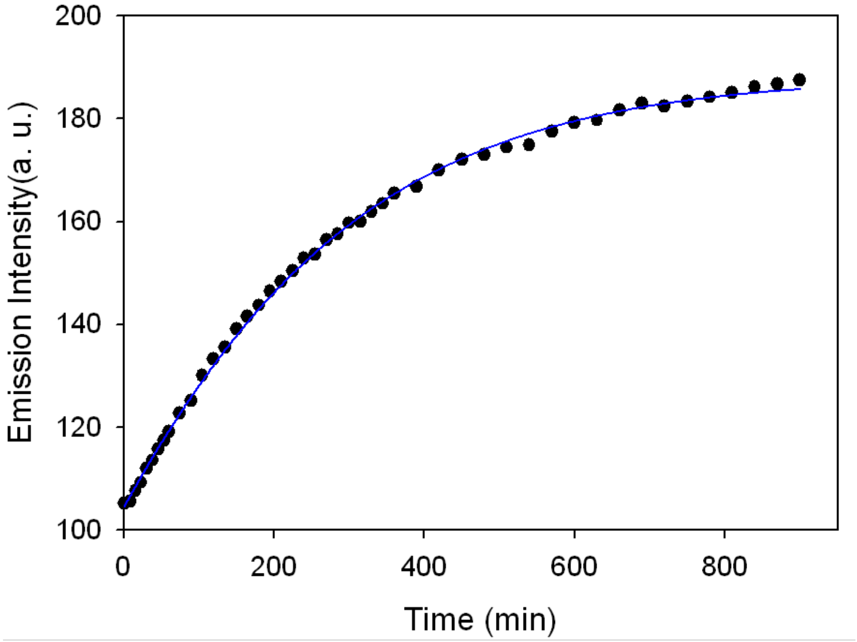

Supplementary Fig. 8. Observation of the dethreading of [**1**⊃*E*-**2**]$^+$. Time-dependent luminescence changes (λ_{exc} = 272 nm, λ_{em} = 390 nm) upon 20-fold dilution of a solution of 75 μM **1** and *E*-$\mathbf{2}^+$ (86% initial complexation) in CH_2Cl_2 at 20 °C. The full line is the data fit according to a first-order kinetic equation.

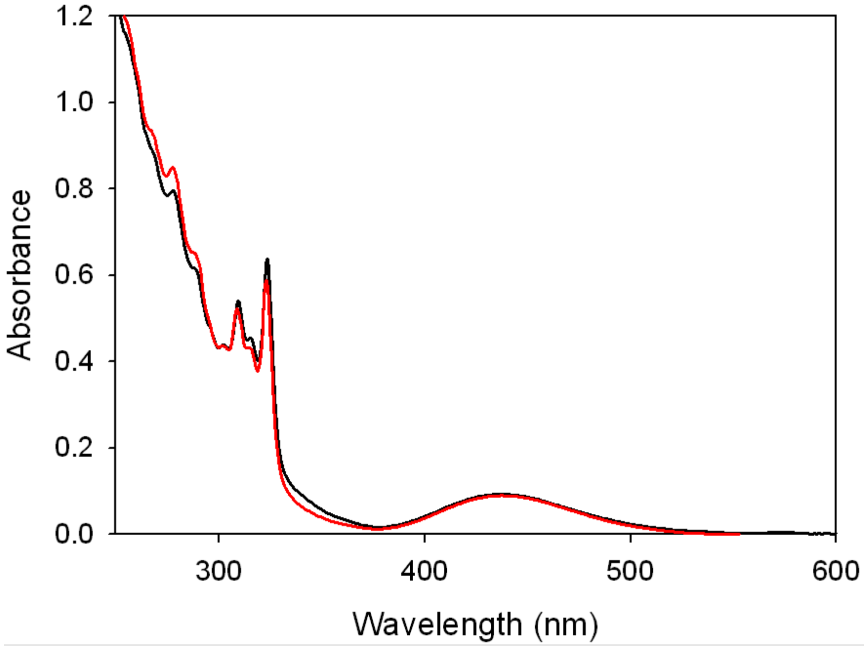

Supplementary Fig. 9. Sum of the absorption spectra of 60 μM **1** and *Z*-**2**$^+$ (black line), and absorption spectrum of the mixture of the two compounds at the same concentration (CH_2Cl_2, r.t.). The sum of the absorption spectra is obtained mathematically from the molar absorption coefficient of the two components, the absorption spectrum of the mixture is obtained upon exhaustive irradiation (365 nm) of an equilibrated mixture of **1** and *Z*-**2**$^+$.

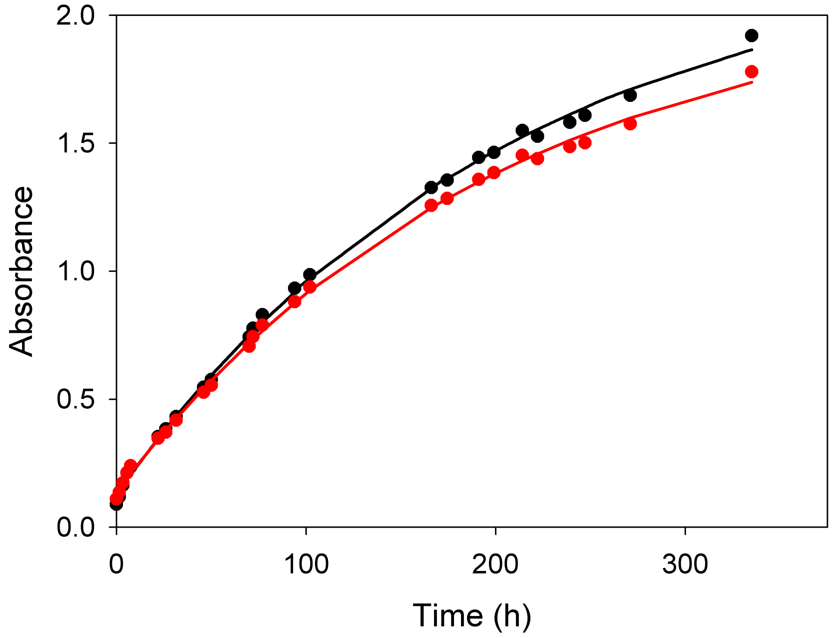

Supplementary Fig. 10. Time-dependent absorption changes at 340 nm observed on a 150 μM CH_2Cl_2 solution of *Z*-**2**$^+$ alone (red circles) and in the presence of 150 μM **1** (black circles) in the dark at 20 °C, highlighting the occurrence of the *Z*→*E* thermal isomerization. The lines are the data fitting according to a first-order kinetic equation.

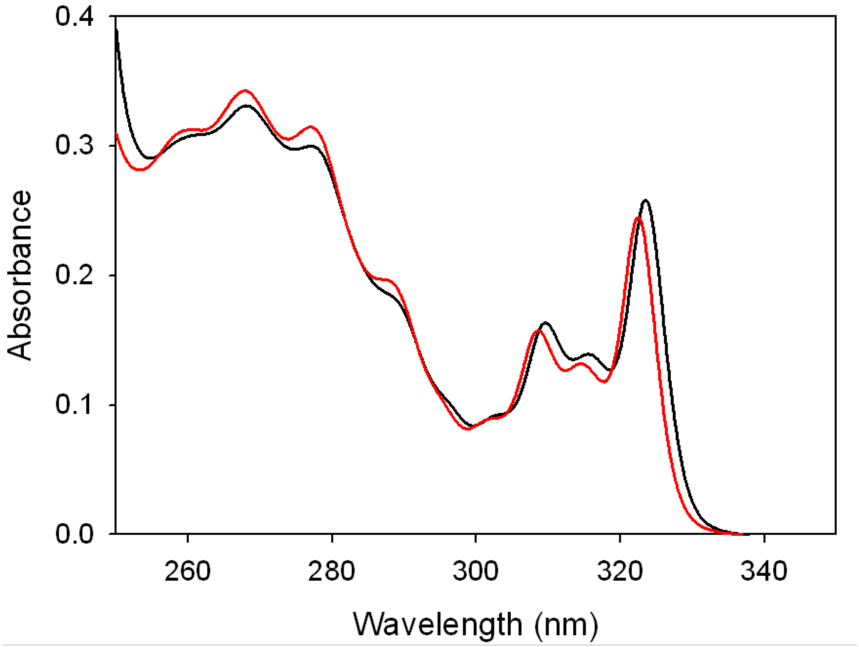

Supplementary Fig. 11. Sum of the absorption spectra of 30 μM **1** and a 1.0 mM **3**$^+$ (black line), and absorption spectrum of the mixture of the two compounds at the same concentration (CH_2Cl_2, r.t.). Dedicated spectrophotometric cells with separated compartments allowed a careful *in situ* determination of the spectra of unmixed and mixed solutions.

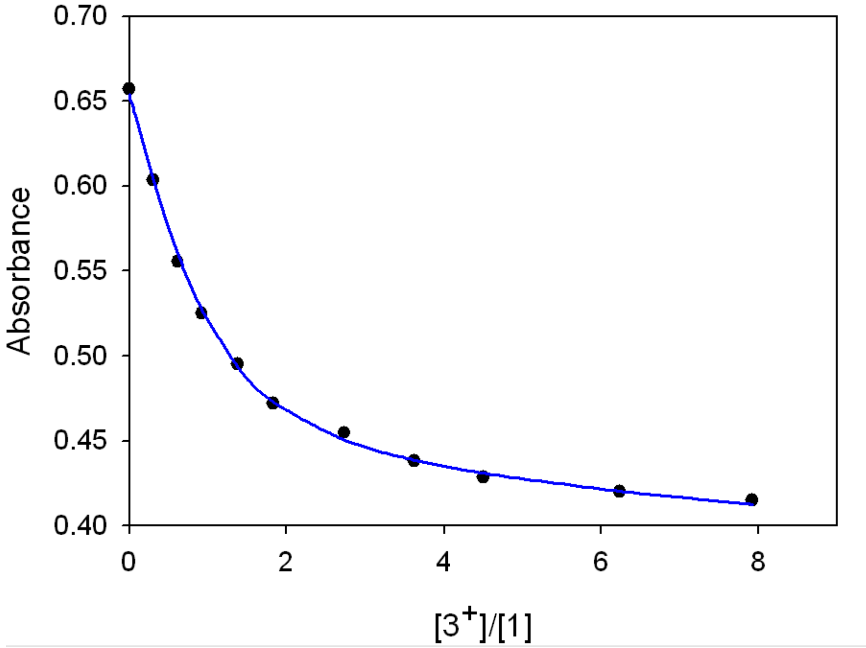

Supplementary Fig. 12. Titration curve, obtained from the absorbance values at 325 nm, observed upon addition of **3**$^+$ to a 80 μM solution of **1** in CH_2Cl_2 at 20 °C. The full line represents the data fitting according to a 1:1 binding model.

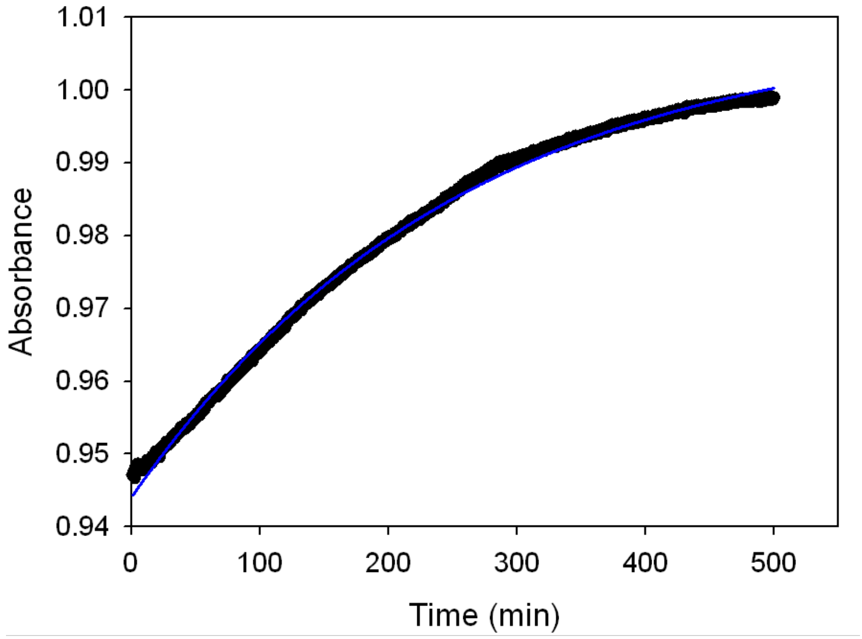

Supplementary Fig. 13. Observation of the dethreading of [**1**⊃**3**]$^+$. Time-dependent absorbance changes at 325 nm upon 6-fold dilution of a solution of 175 µM **1** and **3**$^+$ (66 % initial complexation) in CH_2Cl_2 at 20 °C. The full line is the data fit according to a first-order kinetic equation. To enhance the increase in the absorbance 5 cm pathlength cuvettes were used in this experiment.

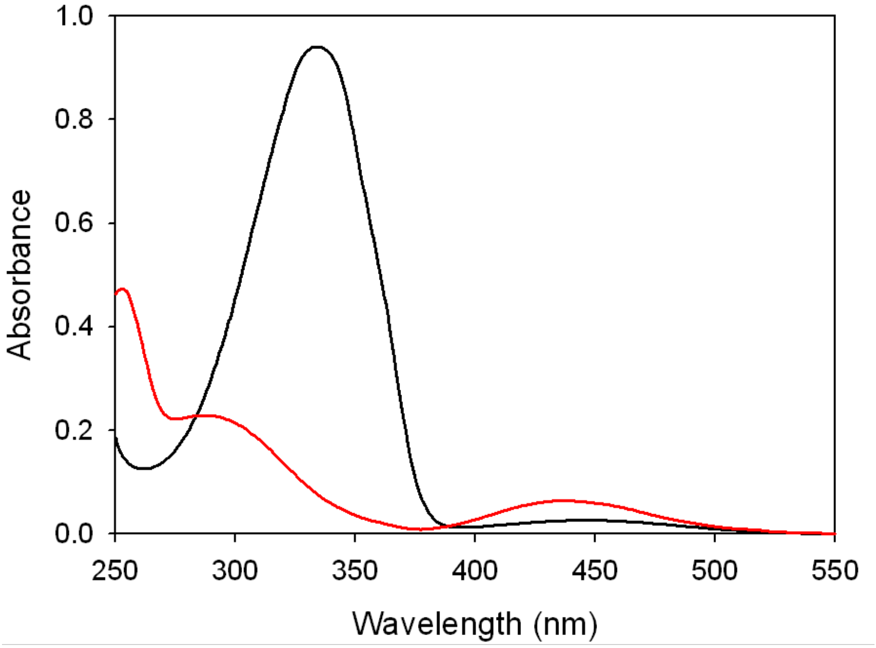

Supplementary Fig. 14. Absorption spectrum of 22 µM *EE*-**4**$^+$ (blue line), and absorption spectrum of *ZZ*-**4**$^+$ (red line), obtained upon exhaustive irradiation of the solution at 365 nm (CH_2Cl_2, r.t.).

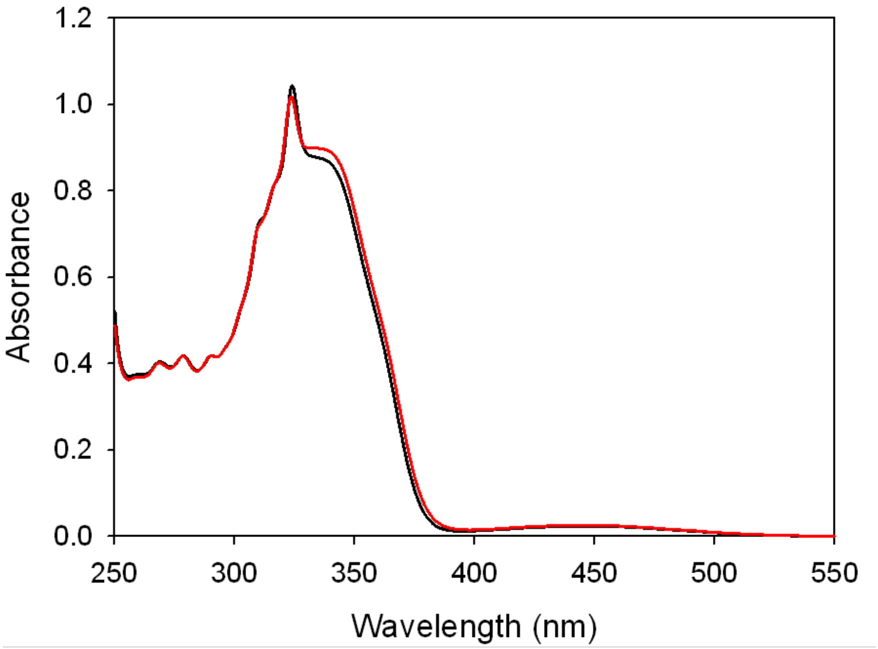

Supplementary Fig. 15. Sum of the absorption spectra of 20 µM **1** and *E*-$\mathbf{4}^+$ (black line), and absorption spectrum of the mixture of the two compounds at the same concentration (CH_2Cl_2, r.t.). Dedicated spectrophotometric cells with separated compartments allowed a careful *in situ* determination of the spectra of unmixed and mixed solutions.

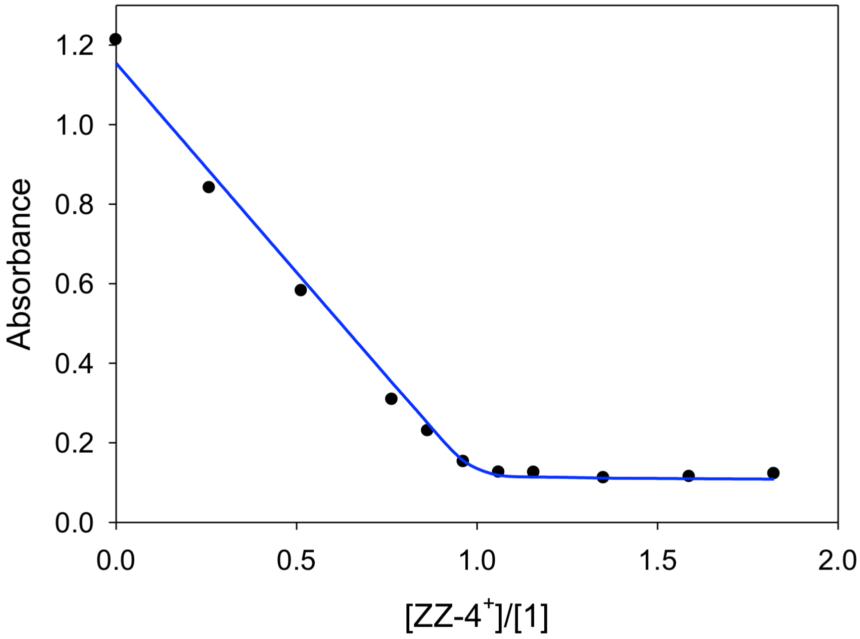

Supplementary Fig. 16. Titration curve, obtained from emission intensity values (λ_{exc} = 282 nm, λ_{em} = 390 nm), observed upon addition of *EE*-$\mathbf{4}^+$ to a 50 µM solution of **1** in CH_2Cl_2 at 20 °C. The full line represents the data fitting according to a 1:1 binding model.

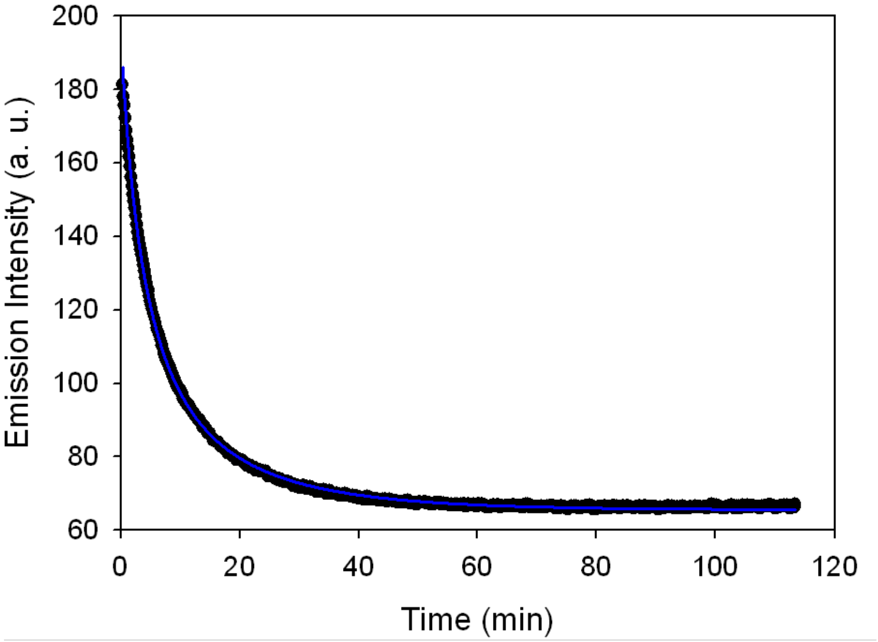

Supplementary Fig. 17. Time-dependent luminescence changes (λ_{exc} = 282 nm, λ_{em} = 390 nm) observed upon mixing 100 μM **1** with 100 μM *EE*-$\mathbf{4}^{+}$ in CH_2Cl_2 at 20 °C. The full line represents the data fitting according to a kinetic model consisting of a second-order threading and an opposed first-order dethreading.

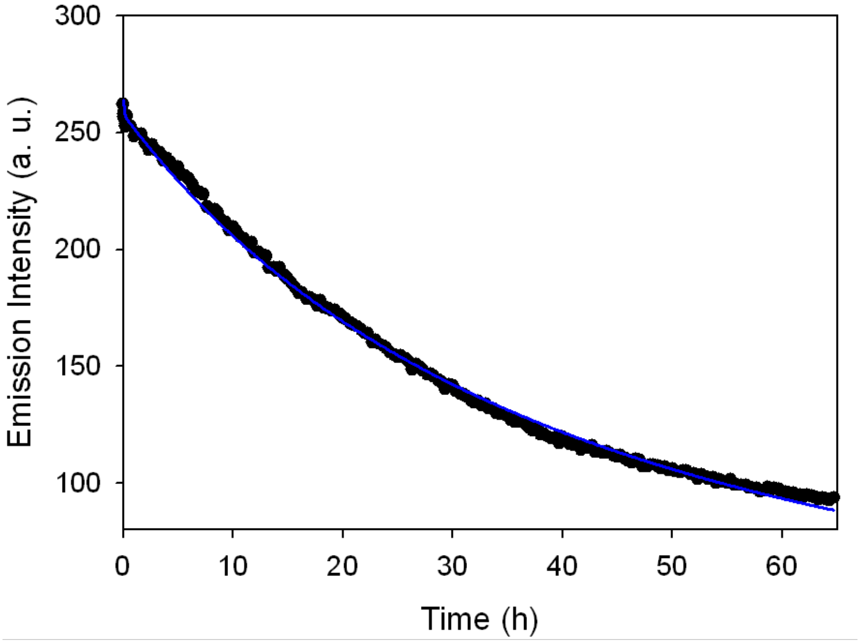

Supplementary Fig. 18. Time-dependent luminescence changes (λ_{exc} = 282 nm, λ_{em} = 390 nm) observed upon mixing 100 μM **1** with 100 μM *ZZ*-$\mathbf{4}^{+}$ in CH_2Cl_2 at 20 °C. The full line represents the data fitting according to a kinetic model consisting of a second-order threading and opposed first-order dethreading and *Z*→*E* isomerization.

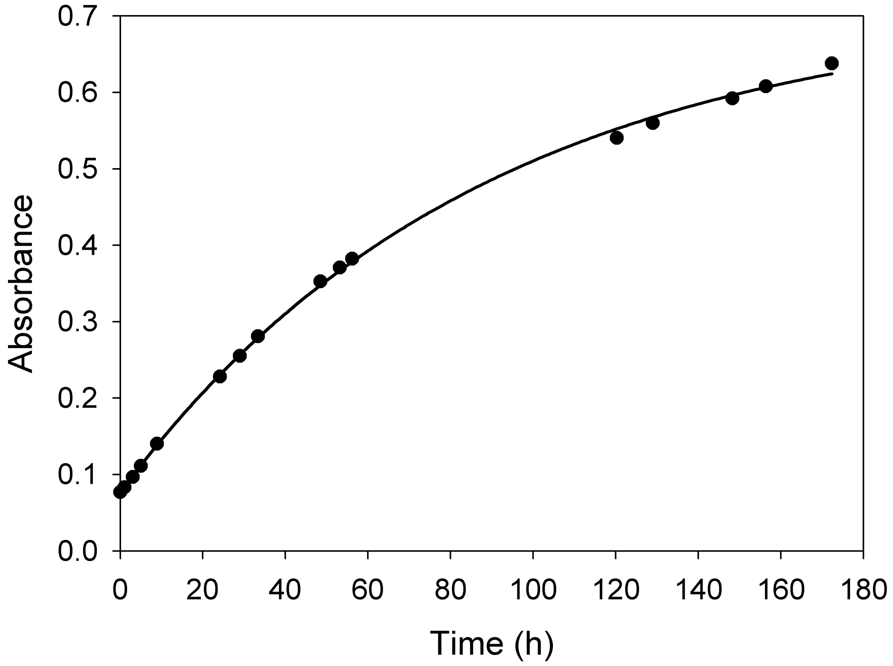

Supplementary Fig. 19. Time-dependent absorption changes at 340 nm observed on a 20 μM CH_2Cl_2 solution of *ZZ*-**4**$^+$ alone (green circles) in the dark at 20 °C, highlighting the occurrence of the *Z*→*E* thermal isomerization. The line is the data fitting according to a first-order kinetic equation.

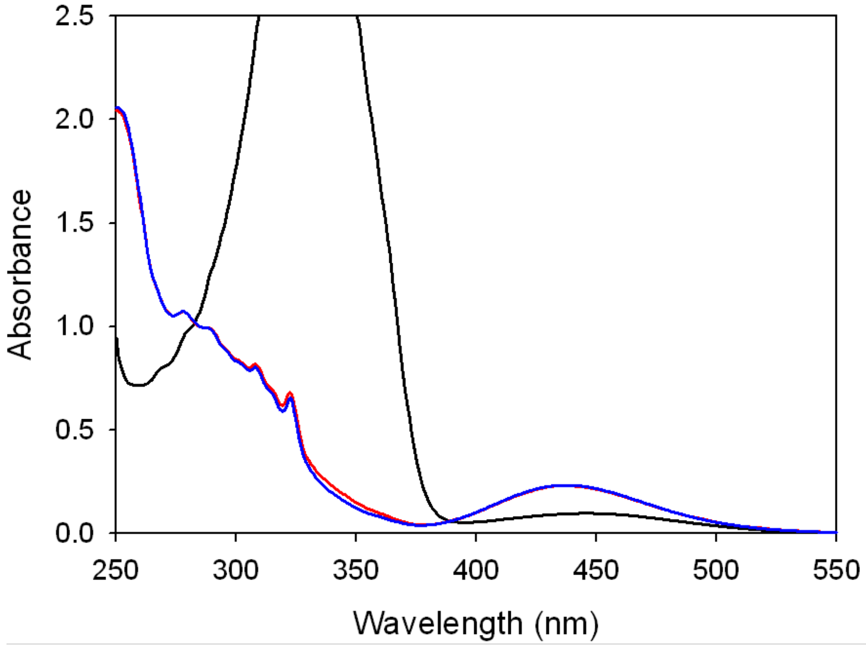

Supplementary Fig. 20. Absorption spectra corresponding to the luminescence data presented in Figure 4. The black line is the absorption spectrum of a solution containing 50 μM **1** and 150 μM *E*-**2**$^+$. Quick (5 min) exhaustive irradiation of this solution at 365 nm generates the spectrum shown as the red line. The blue line is the absorption spectrum after prolonged (3.5 h) low-intensity 365-nm irradiation of the same solution. The absorption spectra recorded at intermediate irradiation times are all superimposed with the blue line and are omitted for clarity.

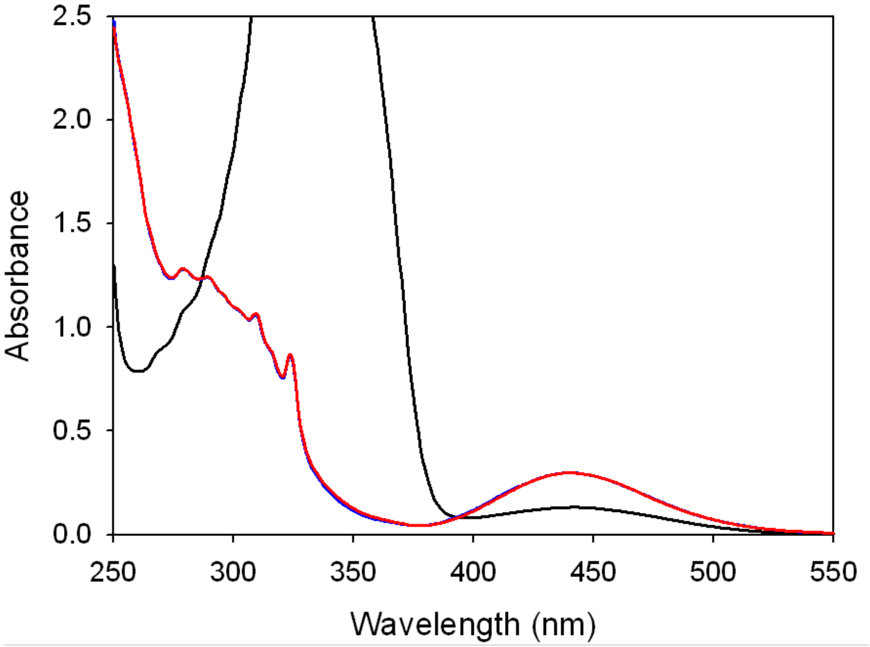

Supplementary Fig. 21. Absorption spectra corresponding to the luminescence data presented in Figure 4 (control experiment). The black line is the absorption spectrum of a solution containing 50 μM **1** and 150 μM deprotonated axle *E*-**2**. Quick (5 min) exhaustive irradiation of this solution at 365 nm generates the spectrum shown as the red line. The blue line is the absorption spectrum after prolonged (3.5 h) low-intensity 365-nm irradiation of the same solution. The absorption spectra recorded at intermediate irradiation times are all superimposed with the blue line and are omitted for clarity.

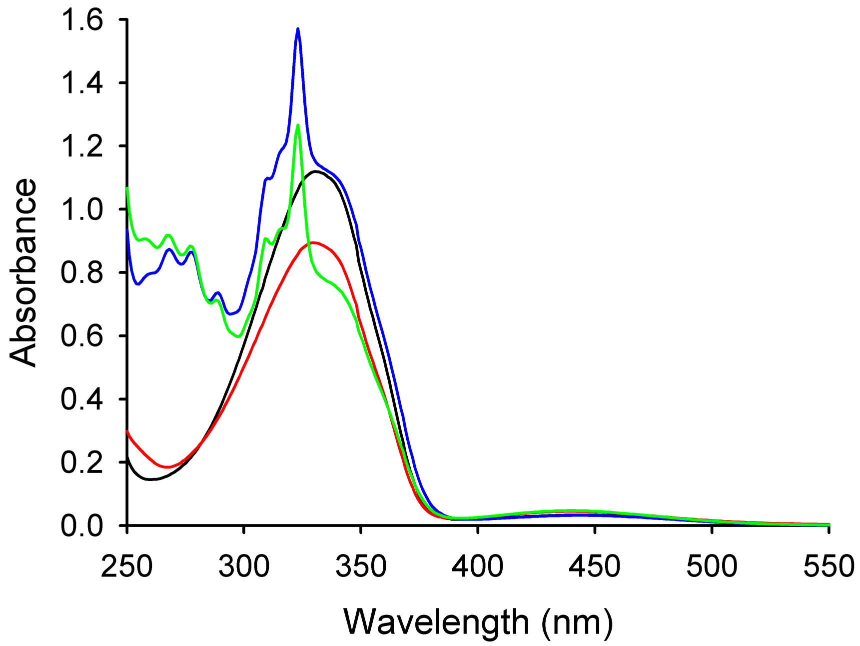

Supplementary Fig. 22. Absorption spectra of 50 μM $\mathbf{2}^+$ in the dark (pure *E*- isomer, black line) and at the photostationary state (λ_{irr} = 287 nm, red line), and absorption spectra of a 50 μM mixture of **1** and $\mathbf{2}^+$ in the dark (pure *E*- isomer, blue line) and at the photostationary state (λ_{irr} = 286 nm, green line) (CH_2Cl_2, r.t.).

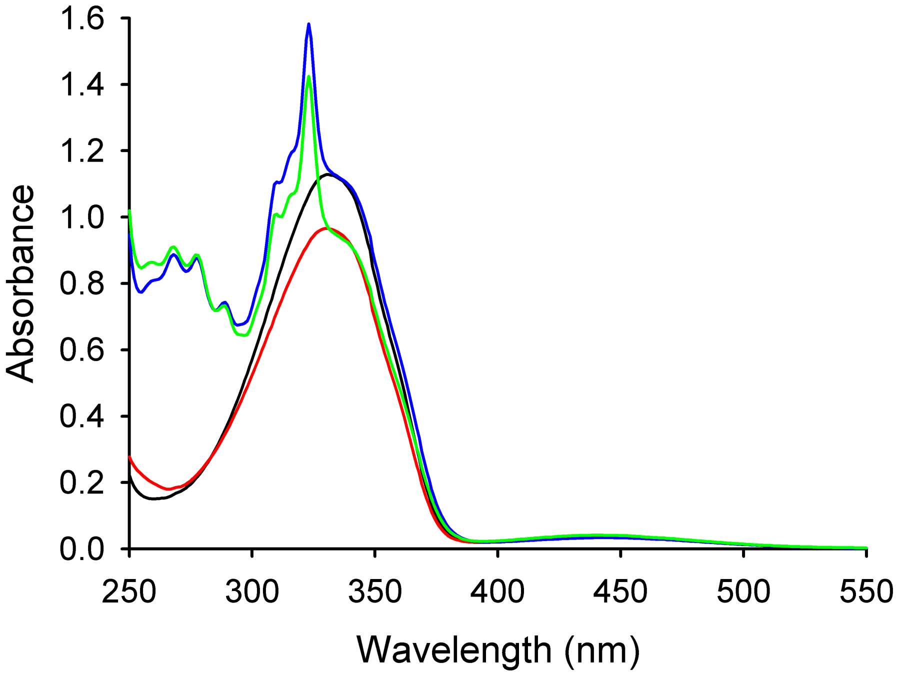

Supplementary Fig. 23. Absorption spectra of 50 μM **2**$^+$ in the dark (pure *E*- isomer, black line) and at the photostationary state (λ_{irr} = 436 nm, red line), and absorption spectra of a 50 μM mixture of **1** and **2**$^+$ in the dark (pure *E*- isomer, blue line) and at the photostationary state (λ_{irr} = 436 nm, green line) (CH_2Cl_2, r.t.).

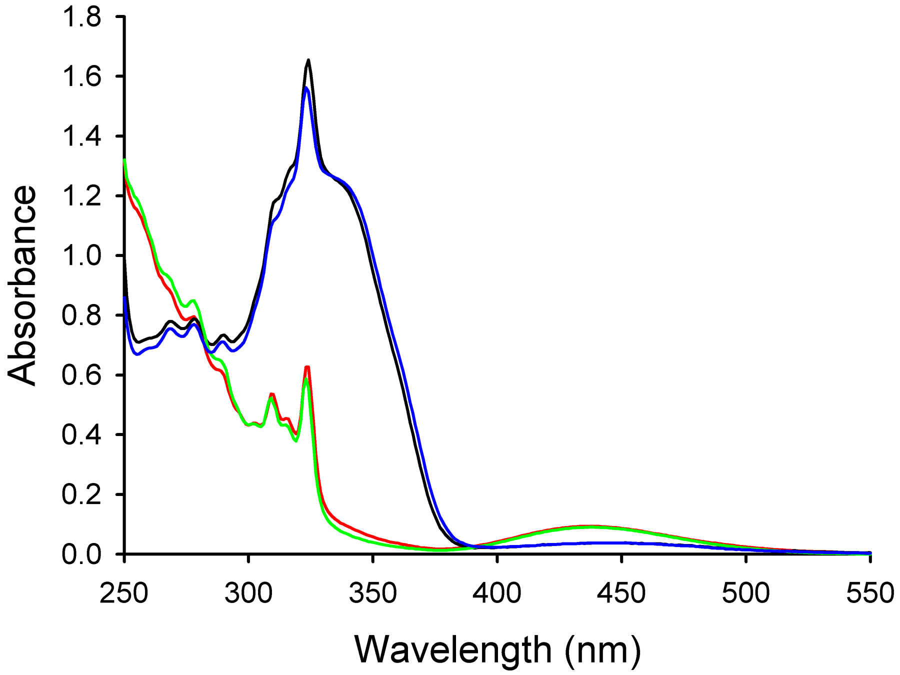

Supplementary Fig. 24. Absorption spectra of the sum of 55 μM **1** and **2**$^+$ in the dark (pure *E*- isomer, black line) and at the photostationary state (λ_{irr} = 365 nm, red line) and absorption spectra of a 55 μM mixture of the two components in the dark (pure *E*- isomer, blue line) and at the photostationary state (λ_{irr} = 365 nm, green line) (CH_2Cl_2, r.t.).

4. References

1. Pedersen, C. J. *J. Am. Chem. Soc.* **89**, 7017 (1969).
2. Baroncini, M., Silvi, S., Venturi, M. & Credi, A. *Angew. Chem. Int. Ed.* **51**, 4223 (2012).
3. Montalti, M., Credi, A., Prodi, L. & Gandolfi, M. T. *Handbook of Photochemistry – Third Edition* (CRC Press, 2006).
4. Binstead, R.A. SPECFIT (Spectrum Software Associates, Chapel Hill, USA, 1996).
5. Credi, A. & Prodi, L. *J. Mol. Struct.*, in press; DOI: 10.1016/j.molstruc.2014.03.028.
6. Klán, P. & Wirz, J. *Photochemistry of Organic Compounds: From Concepts to Practice* (Wiley, New York, 2009) p. 117.
7. Astumian, R. D. *Phys. Chem. Chem. Phys.* **9**, 5067 (2007).
8. Coskun, A., Banaszak, M., Astumian, R. D., Stoddart, J. F. & Grzybowski, B. A. *Chem. Soc. Rev.* **41**, 19 (2012).